Longitudinal fluid–dynamics for ultrarelativistic heavy–ion collisions

L.M. Satarov [a,b], A.V. Merdeev [b], I.N. Mishustin [a,b] and H. Stöcker [a]

[a] *Frankfurt Institute for Advanced Studies, J.W. Goethe University, Max–von–Laue–Str. 1, D–60438 Frankfurt am Main, Germany*

[b] *The Kurchatov Institute, Russian Research Center, 123182 Moscow, Russia*

Abstract

We develop a 1+1 dimensional hydrodynamical model for central heavy–ion collisions at ultrarelativistic energies. Deviations from Bjorken's scaling are taken into account by implementing finite–size profiles for the initial energy density. The calculated rapidity distributions of pions, kaons and antiprotons in central Au+Au collisions at $\sqrt{s_{NN}} = 200\,\mathrm{GeV}$ are compared with experimental data of the BRAHMS Collaboration. The sensitivity of the results to the choice of the equation of state, the parameters of initial state and the freeze–out conditions is investigated. The best fit of experimental data is obtained for a soft equation of state and Gaussian–like initial profiles of the energy density.

Key words: hydrodynamics, equation of state, pions
PACS: 12.38.Mh, 24.10.Nz, 25.75.-q, 25.75.Nq

High–energy heavy–ion collisions provide a unique tool for studying properties of hot and dense strongly–interacting matter in the laboratory. The theoretical description of such collisions is often done within the framework of a hydrodynamic approach. This approach opens the possibility to study the sensitivity of collision dynamics and secondary particle distributions to the equation of state (EOS) of the produced matter. The two most famous realizations of this approach, which differ by the initial conditions, have been proposed by Landau [1] (full stopping) and Bjorken [2] (partial transparency). In recent decades many versions of the hydrodynamic model were developed ranging from simplified 1+1 [3,4,5,6] and 2+1 dimensional models [6,7,8,9,10,11] of the Landau or Bjorken type to more sophisticated 3+1 dimensional models [12,13,14,15,16,17]. One should also mention the multi–fluid models [18,19,20,21,22,23,24] which consider the whole collision process including the nuclear interpenetration stage. Recent theoretical investigations show that fluid–dynamical models

give a very good description of many observables at the SPS and RHIC bombarding energies (see e.g. Ref. [25]).

The 2+1 dimensional hydrodynamical models have been successfully applied [7,8,9,10,11] to describe the p_T distributions of mesons and their elliptic flow at midrapidity. These models assume a boost–invariant expansion [2] of matter in the longitudinal (beam) direction and, therefore, cannot explain experimental data in a broad rapidity region, where strong deviations from the scaling regime have been observed. More realistic 3+1 dimensional fluid–dynamical simulations have been already performed for heavy–ion collisions at SPS and RHIC energies. But as a rule, the authors of these models do not study the sensitivity of the results to the choice of initial and final (freeze–out) stages. On the other hand, it is not clear at present, which initial conditions, Landau–like [1] or Bjorken–like [2], are more appropriate for ultrarelativistic collisions.

Our main goal in this paper is to see how well the fluid–dynamical approach describes the RHIC data on $\pi, K, \overline{p}$ distributions over a broad rapidity interval, reported recently by the BRAHMS Collaboration [26,27]. Within our approach we explicitly impose a constraint on the total energy of the produced particles which follows from these data.

Below we study the evolution of highly excited, and possibly deconfined, strongly–interacting matter produced in ultrarelativistic heavy–ion collisions. It is assumed that after a certain thermalization stage this evolution can be described by the ideal relativistic hydrodynamics. The energy–momentum tensor is written in a standard form [1]

$$T^{\mu\nu} = (\epsilon + P) U^\mu U^\nu - P g^{\mu\nu}, \tag{1}$$

where ϵ, P and U^μ are the rest–frame energy density, pressure and the collective 4–velocity of the fluid.

We consider central collisions of equal nuclei disregarding the effects of transverse collective expansion. It is convenient to parametrize U^μ in terms of the longitudinal flow rapidity Y as $U^\mu = (\cosh Y, \mathbf{0}, \sinh Y)^\mu$. All calculations are performed using the light–cone variables [2], namely, the proper time τ and the space–time rapidity η, defined as

$$\tau = \sqrt{t^2 - z^2}, \quad \eta = \tanh^{-1}\left(\frac{z}{t}\right) = \frac{1}{2}\ln\frac{t+z}{t-z}. \tag{2}$$

In these coordinates, the equations of relativistic hydrodynamics, $\partial_\nu T^{\mu\nu} = 0$, for an ideal baryon–free fluid take the following form [28]

[1] Units with $\hbar = c = 1$ are used throughout the paper.

$$\left(\tau\frac{\partial}{\partial\tau}+\tanh(Y-\eta)\frac{\partial}{\partial\eta}\right)\epsilon+(\epsilon+P)\left(\tanh(Y-\eta)\tau\frac{\partial}{\partial\tau}+\frac{\partial}{\partial\eta}\right)Y=0\,, \quad (3)$$

$$(\epsilon+P)\left(\tau\frac{\partial}{\partial\tau}+\tanh(Y-\eta)\frac{\partial}{\partial\eta}\right)Y+\left(\tanh(Y-\eta)\tau\frac{\partial}{\partial\tau}+\frac{\partial}{\partial\eta}\right)P=0\,. \quad (4)$$

To solve Eqs. (3)–(4), one needs to specify the EOS, $P=P(\epsilon)$, and the initial profiles $\epsilon(\tau_0,\eta)$ and $Y(\tau_0,\eta)$ at a time $\tau=\tau_0$ when the fluid may be considered as thermodynamically equilibrated.

Following Ref. [15], we choose the initial conditions for a finite-size fluid, generalizing the Bjorken scaling conditions:

$$Y(\tau_0,\eta)=\eta, \quad \epsilon(\tau_0,\eta)=\epsilon_0\exp\left[-\frac{(|\eta|-\eta_0)^2}{2\sigma^2}\Theta(|\eta|-\eta_0)\right], \quad (5)$$

where $\Theta(x)\equiv(1+\mathrm{sgn}\,x)/2$. The particular choice $\eta_0=0$ corresponds to the pure Gaussian profile of the energy density. At small σ such a profile can be similar to the Landau initial condition [2]. On the other hand, when σ or η_0 tends to infinity, one gets the limiting case of the Bjorken scaling solution. Below we adopt the value $\tau_0=1\,\mathrm{fm/c}$.

The deconfinement phase transition is implemented through a bag–like EOS in the parametrization suggested in Ref. [11]. This EOS consists of three parts, denoted below by indices H, M and Q corresponding, respectively, to the hadronic, "mixed" and quark–gluon phases. In the case of equilibrated baryon–free matter the pressure P, energy density ϵ and entropy density s may be regarded as functions of the temperature only. The hadronic phase consists of pions, kaons, meson resonances and baryon–antibaryon pairs. It corresponds to the domain of low energy densities, $\epsilon<\epsilon_H$, and temperatures, $T<T_H$. The sound velocity, $c_s=\sqrt{dP/d\epsilon}$, is assumed to be constant ($c_s=c_H$) in this phase:

$$P=c_H^2\epsilon\,,\ T=T_H\left(\frac{\epsilon}{\epsilon_H}\right)^{\frac{c_H^2}{1+c_H^2}} \quad (\epsilon<\epsilon_H)\,. \quad (6)$$

The mixed phase corresponds to intermediate energy densities, from ϵ_H up to ϵ_Q. The following parametrization is used for this region:

$$P=c_M^2\epsilon-(1+c_M^2)\,B_M\,,\ T=T_H\left(\frac{\epsilon-B_M}{\epsilon_H-B_M}\right)^{\frac{c_M^2}{1+c_M^2}} \quad (\epsilon_H<\epsilon<\epsilon_Q)\,. \quad (7)$$

[2] Within the Landau model [1] $\sigma\propto\gamma^{-1}$ and $\epsilon_0\propto\gamma^2$ where γ is the c.m. Lorentz–factor of colliding nuclei.

Table 1
Parameters of EOS with the deconfinement phase transition.

$\epsilon_H\,(\mathrm{GeV/fm^3})$	$\epsilon_Q\,(\mathrm{GeV/fm^3})$	c_H^2	c_M^2	c_Q^2	$T_H\,(\mathrm{MeV})$	$T_Q\,(\mathrm{MeV})$	$B_M\,(\mathrm{MeV/fm^3})$	$B_Q\,(\mathrm{MeV/fm^3})$
0.45	1.65	0.15	0.02	1/3	165	169	−57.4	344

Here B_M is the bag constant, determined from the condition of continuity of $P(\epsilon)$ at $\epsilon = \epsilon_H$. Due to the small sound velocity c_M (see Table 1), both pressure and temperature increase only weakly with ϵ in the mixed phase region. The third, quark–gluon plasma region of the EOS corresponds to $\epsilon > \epsilon_Q$. The expressions for $P(\epsilon)$ and $T(\epsilon)$ in this region can be obtained from Eq. (7) by replacing H, M by indices Q. The corresponding formulae for the entropy density are obtained from the thermodynamic relation $s = (\epsilon + P)/T$. Our parameters $\epsilon_H, \epsilon_Q, c_H^2, c_M^2, c_Q^2, T_H$ are close to those used in Refs. [7,11]. The parameters B_M, B_Q, T_Q are found from the continuity conditions for P and T. Unless stated otherwise, this EOS is used in the calculations presented in this paper. To study the sensitivity to the EOS, we have performed also calculations for several purely hadronic EOSs. In this case we extend Eq. (6) to all energy densities, taking the same ϵ_H, T_H as in Table 1, but choosing different c_H^2 from 1/10 to 1/3.

Using the equations of fluid dynamics one can show that the total energy and entropy of the fluid can be expressed as

$$E = \int d\sigma_\mu T^{\mu 0} = S_\perp \tau_0 \int\limits_{-\infty}^{+\infty} d\eta \left[\epsilon \cosh Y \cosh\left(Y-\eta\right) + P \sinh Y \sinh\left(Y-\eta\right)\right], \quad (8)$$

$$S = \int d\sigma_\mu s U^\mu = S_\perp \tau_0 \int\limits_{-\infty}^{+\infty} d\eta\, s \cosh\left(Y-\eta\right), \quad (9)$$

where $S_\perp$ is the transverse area of the fluid. The r.h.s. of Eqs. (8)–(9) give the values of the energy and entropy at $\tau = \tau_0$. Equations (8) and (9) can be considered as sum rules for the total energy and entropy of the produced particles. Below we use Eq. (8) to constrain possible values of the parameters characterizing the initial state. This is possible since the total energy of produced particles is known from experimental data [26].

The numerical solution of Eqs. (3)–(4) is obtained by using the relativistic version [29] of the flux–corrected transport algorithm [30]. We have checked that our numerical code conserves the total energy E and entropy S at any hypersurface σ_μ lying above the initial hyperbola $\tau = \tau_0$, on the level better than 1% even for $\tau \gtrsim 200\,\mathrm{fm/c}$.

The momentum spectra of secondary hadrons are calculated by applying the standard Cooper–Frye formula [31], assuming that particles are emitted with-

out further rescatterings from elements $d\sigma_\mu$ of the freeze–out hypersurface $\tau = \tau_F(\eta)$. Then, the invariant momentum distribution for each particle species is given by the expression

$$E\frac{d^3N}{d^3p} = \frac{d^3N}{dy\,d^2p_T} = \frac{g}{(2\pi)^3}\int d\sigma_\mu p^\mu \left\{\exp\left(\frac{p_\nu U_F^\nu - \mu_F}{T_F}\right) \pm 1\right\}^{-1}, \qquad (10)$$

where p^μ is the 4–momentum of the particle, y and $\boldsymbol{p}_T$ are, respectively, its longitudinal rapidity and transverse momentum, g denotes the particle's statistical weight. The subscript F in the collective 4–velocity U^μ, temperature T and chemical potential μ implies that these quantities are taken on the freeze–out hypersurface [3]. The plus or minus sign in the r.h.s. of Eq. (10) correspond to fermions or bosons, respectively.

For a cylindrical fireball of radius R expanding only in the longitudinal direction, one can write $S_\perp = \pi R^2$ and $d\sigma^\mu = \pi R^2 (dz, \mathbf{0}, dt)^\mu$. Using Eq. (2) one arrives at the following relation

$$d\sigma_\mu p^\mu = \pi R^2 m_T \left\{\tau_F(\eta)\cosh(y-\eta) - \tau_F'(\eta)\sinh(y-\eta)\right\} d\eta\,. \qquad (11)$$

Here m_T is the particle's transverse mass defined as $m_T = \sqrt{m^2 + \boldsymbol{p}_T^2}$, where m is the corresponding vacuum mass. In the same approximation one can also write the expression

$$p_\nu U_F^\nu = m_T \cosh(y - Y_F(\eta))\,, \qquad (12)$$

where $Y_F(\eta) = Y(\tau_F(\eta), \eta)$. An explicit expression for particle spectra at freeze–out is obtained after substituting (11)–(12) into Eq. (10) and integrating over η from $-\infty$ to $+\infty$. Note that Bjorken's model [2] corresponds to $Y_F = \eta$ and τ_F, T_F independent of η. As can be seen from Eqs. (10)–(12), the rapidity distributions of all particles should be flat in this case.

We adopt the freeze–out condition, assuming that a given fluid element decouples from the rest of the fluid when its temperature decreases below a certain value T_F. For finite–size initial conditions, $T(\tau_0, \eta) \to 0$ at $|\eta| \to \infty$, so that the fluid elements at large $|\eta|$ have temperatures below T_F from the very beginning, i.e. at $\tau = \tau_0$. We treat these elements as decoupled instantaneously ($\tau_F = \tau_0$) and use in Eq. (10) the initial values of Y and T instead of Y_F and T_F. Direct calculation shows, that such elements contribute only little to the tails of the rapidity distributions. The value of T_F is considered as an

[3] Below we assume that the chemical and thermal freeze–out hypersurfaces coincide. In this case $\mu_F = 0$ for baryon–free matter.

adjustable model parameter which is found from the best fit to experimental data.

Below we show the results for rapidity distributions of π– and K–mesons as well as antiprotons produced in central Au+Au collisions at $\sqrt{s_{NN}} = 200\,\mathrm{GeV}$. In all calculations we use the fireball radius $R = 6.5\,\mathrm{fm}$. The results are compared with data of the BRAHMS Collaboration [26,27] for most central (0%–5%) collisions.

In calculating these distributions one should take into account not only directly produced particles but also feeding from resonance decays. Below we assume that the freeze–out temperatures for directly produced particles and corresponding resonances are the same. One of the most important contributions to the pion yield is given by $\rho(770)$–mesons. The spectrum of π^+–mesons originating from these decays is calculated by using the expression [32]

$$E_\pi \frac{d^3N_{\rho\to\pi^+}}{d^3p} = \frac{1}{3\pi} \int\limits_{2m_\pi}^{\infty} \frac{dm_R\, w(m_R)}{\sqrt{m_R^2 - 4m_\pi^2}} \int d^3p_R \frac{d^3N_R}{d^3p_R}\, \delta\left(\frac{pp_R}{m_R} - \frac{m_R}{2}\right), \qquad (13)$$

where the first integration corresponds to averaging over the mass spectrum of ρ–mesons, p_R and p are, respectively, the 4–momenta of the ρ–resonance and of the secondary pion. The normalization coefficient in Eq. (13) takes into account that the number of π^+–mesons produced in ρ–decays equals 2/3 of the total multiplicity of ρ–mesons. The freeze–out momentum spectrum of ρ–mesons, d^3N_R/d^3p_R, is calculated using Eqs. (10)–(12) with $m = m_R$, $g = g_\rho = 9$. We use the parametrization of the ρ–meson mass distribution, $w(m_R)$, suggested in Ref. [32].

The feeding of the pion yields from other meson and baryon resonances ($R = \eta$, $\omega, K^*, \Delta \ldots$) is obtained in the zero–width approximation, assuming that the contribution of the resonance R is proportional to its equilibrium density $n_R(T_F)$, multiplied by a factor d_R, the average number of π^+ mesons produced in this resonance decay ($d_\rho = 2/3, d_\eta = 0.65 \ldots$). The details of n_R and d_R calculations can be found in Ref. [33]. We have checked for several resonances with two–body decays (e.g. for $R = K^*$) that such a procedure yields a very good accuracy. As a result, we get the following formula for the total resonance contribution to the spectrum of π^+ mesons:

$$\sum_R \frac{d^3N_{R\to\pi^+}}{dy\, d^2p_T} = \alpha \frac{d^3N_{\rho\to\pi^+}}{dy\, d^2p_T}, \qquad (14)$$

where the enhancement factor α is defined as follows

$$\alpha = \sum_R \frac{d_R}{d_\rho} \frac{n_R(T_F)}{n_\rho(T_F)}. \qquad (15)$$

We include meson (baryon and antibaryon) resonances with masses up to 1.3 (1.65) GeV and widths $\Gamma < 150$ MeV. The statistical weights, masses and branching ratios of these resonances are taken from Ref. [34] . The factor α decreases gradually with decreasing freeze–out temperature: $\alpha = 3.0, 2.4, 2.3$ for $T_F = 165, 130, 100\,\mathrm{MeV}$, respectively.

When calculating the kaon spectra we explicitly include feeding from decays of $K^*(892)$ (in the zero–width approximation). Higher resonances ($R = \phi, K_1 \ldots$) are taken into account by applying the same procedure as for pions. In this case the enhancement factor changes from 1.5 to 1.2 when T_F goes from 165 to 100 MeV.

In order to reduce the freedom in choosing the initial conditions, we use as an additional constraint the value of the total energy loss, $\Delta E = 73 \pm 6$ GeV per nucleon, deduced from the measurements of the net baryon rapidity distribution in the most central Au+Au collisions [26]. This gives an estimate of the total energy of secondaries in the considered reaction:

$$E = N_{\mathrm{part}}\, \Delta E \simeq 26.1\,\mathrm{TeV}\,, \tag{16}$$

where $N_{\mathrm{part}} \simeq 357$ is the mean number of participating nucleons. Substituting the parametrization (5) into Eq. (8) and taking the value of E from Eq. (16), one gets the relation between the parameters $\epsilon_0, \eta_0, \sigma$.

We have considered different profiles of the initial energy density, ranging from the Gaussian–like ($\eta_0 = 0$) to the table–like ($\sigma = 0$). We found that it is not possible to reproduce the BRAHMS data on the pion and kaon rapidity spectra in Au+Au collisions by choosing either too small ($\epsilon_0 \lesssim 5\,\mathrm{GeV/fm^3}$) or too large ($\epsilon_0 \gtrsim 15\,\mathrm{GeV/fm^3}$) initial energy densities. In these regions the pion and kaon yields can not be reproduced with any T_F . It is also found that the quality of fits is noticeably reduced for initial energy density profiles with sharp edges, corresponding to $\sigma < 1$. As follows from the constraint (16), such profiles should have a very large ϵ_0 or a significant plateau $-\eta_0 < \eta < \eta_0$. This would lead to more flat rapidity distributions of pions and kaons as compared to the BRAHMS data.

A few parameter sets which lead to good fits are listed in Table 2. In all these sets we use the EOS with the phase transition. The sensitivity of the fits to the choice of freeze–out temperature is demonstrated in Figs. 1 and 2 for the parameter set C. The other two sets from Table 2 give very similar rapidity distributions for both pions and kaons. In these calculations we choose various ϵ_0 and σ and determine η_0 from the total energy constraint (16). The best fit of the pion spectrum is achieved for freeze–out temperatures around

Table 2
Parameters of the initial states which give the best fits of the pion, kaon and antiproton rapidity spectra observed in central Au+Au collisions at $\sqrt{s_{NN}} = 200\,\mathrm{GeV}$. T_0 denotes the maximum temperature at $\tau = \tau_0$. E_1 and E_3 are total energies of produced particles within the rapidity intervals $|y| < 1$ and $|y| < 3$, respectively.

set	$\epsilon_0\,(\mathrm{GeV/fm^3})$	σ	η_0	$T_0\,(\mathrm{MeV})$	$E_1\,(\mathrm{TeV})$	$E_3\,(\mathrm{TeV})$	$E/S\,(\mathrm{GeV})$
A	8	1.30	1.14	263	1.49	9.55	0.86
B	9	1.50	0.62	271	1.54	9.59	0.86
C	10	1.74	0	279	1.53	9.25	0.89

$T_F \simeq 130$ MeV [4]. On the other hand, the kaon spectrum can be well reproduced assuming that kaons decouple at the very beginning of the hadronic stage, i.e. at $T_F \simeq 165\,\mathrm{MeV}$. The contribution of resonance decays turns out to be rather significant, especially in the central rapidity region, where it amounts to about 35% (45%) of the total pion (kaon) yield. It is interesting that the initial states A–C have approximately the same total entropy $S \simeq 3 \cdot 10^4$. As one can see from the last column of Table 2, the corresponding E/S–ratios fall into a narrow interval $0.86 - 0.89\,\mathrm{GeV}$.

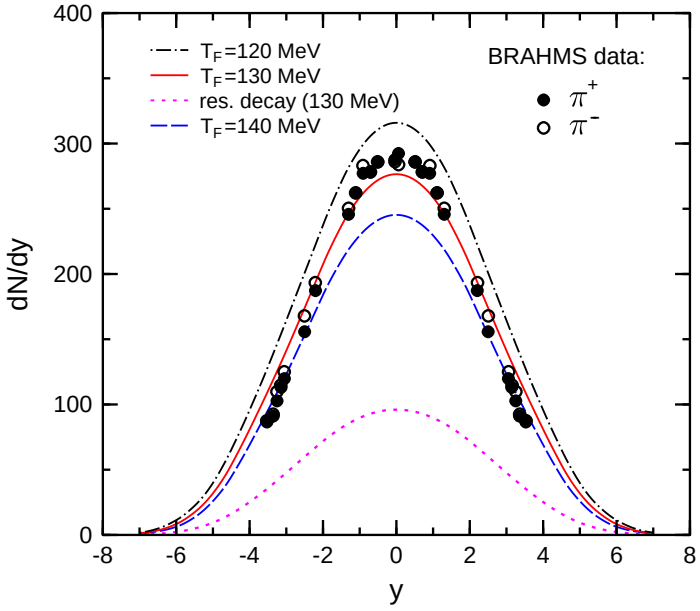

Fig. 1. Rapidity distribution of π^+–mesons in central Au+Au collisions at $\sqrt{s_{NN}} = 200\,\mathrm{GeV}$. Shown are results corresponding to the initial conditions (5) with the parameters $\epsilon_0 = 10\,\mathrm{GeV/fm^3}$, $\eta_0 = 0$, $\sigma = 1.74$. The solid, dashed and dashed–dotted curves correspond to different values of the freeze–out temperature T_F. The dotted line shows contribution of resonance decays in the case $T_F = 130\,\mathrm{MeV}$. Experimental data are taken from Ref. [27].

[4] We did not try to achieve a perfect fit of BRAHMS data, bearing in mind that their systematic errors are quite big, about 15% in the rapidity region $|y| > 1.3$ [27].

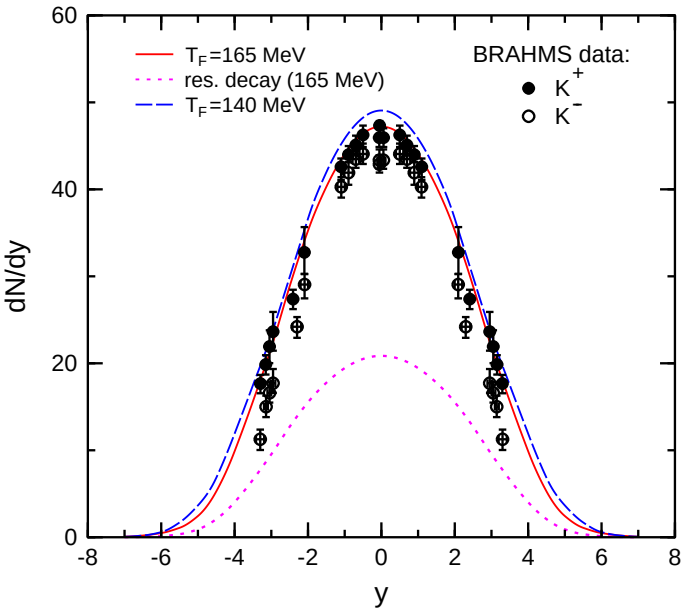

Fig. 2. Same as Fig. 1, but for K^+ rapidity distributions.

As one can see from Fig. 1, the model predicts larger yields of secondary pions for smaller freeze–out temperatures. A much weaker sensitivity to T_F is found for kaons (see Fig. 2). This difference can be explained by the large difference between the pion and the kaon masses. Indeed, in the case of direct pions a good approximation at $T_F > 100\,\mathrm{MeV}$ is to replace the transverse mass m_T in Eqs. (10)–(12) by the pion transverse momentum p_T. Neglecting the second term in the r.h.s. of Eq. (11), one can show that the rapidity distribution of pions at $y = 0$ is proportional to $\xi = \tau_F \cosh\eta\, T_F^3/\cosh^3 Y_F$ integrated over all η. For a rough estimate, one can use the Bjorken relations [2] $Y_F = \eta$, $s_F\tau_F = s_0\tau_0$, where s_F is the entropy density at $T = T_F$. Using Eq. (6) one gets $\tau_F \propto s_F^{-1} \propto T_F^{-1/c_H^2}$ and therefore, $\xi \propto T_F^{3-1/c_H^2}$. This shows that the pion yield grows with decreasing T_F at $c_H^2 < 1/3$. Qualitatively one can say that at low enough c_H the increase of the spatial volume at freeze–out compensates for the decrease of the pion occupation numbers at smaller T_F. This effect is somewhat reduced because of decreasing resonance contributions at smaller temperatures. It is obvious that for kaons this effect should be much weaker due to the presence of the activation exponent $\exp(-m_K/T_F)$. In fact the detailed calculation for the same initial states as in Fig. 2 shows that the kaon yield changes nonmonotonically: it slightly increases when temperature goes from 165 to 140 MeV, but then starts to decrease at lower T_F.

In order to study the sensitivity of the results to the EOS, we have performed calculations using the same initial conditions as before, but applying the hadronic EOS (6) for all stages of the reaction, including the high density phase. Our analysis shows that for soft hadronic EOS with $c_H^2 \lesssim 0.2$ it is

possible to reproduce the observed pion and kaon data with approximately the same quality of the fits as in the calculations with the quark–gluon phase transition. Furthermore, the corresponding freeze–out temperatures do not change significantly. However, we could not achieve satisfactory fits for the "hard" hadronic EOS with $c_H^2 \geqslant 1/3$. These EOS lead to too wide rapidity distributions for both pions and kaons. The reason is that the higher pressure gives a stronger push to the matter in forward and backward directions. From these findings we conclude that the pion and kaon rapidity distributions are consistent with a rather soft EOS at high energy densities.

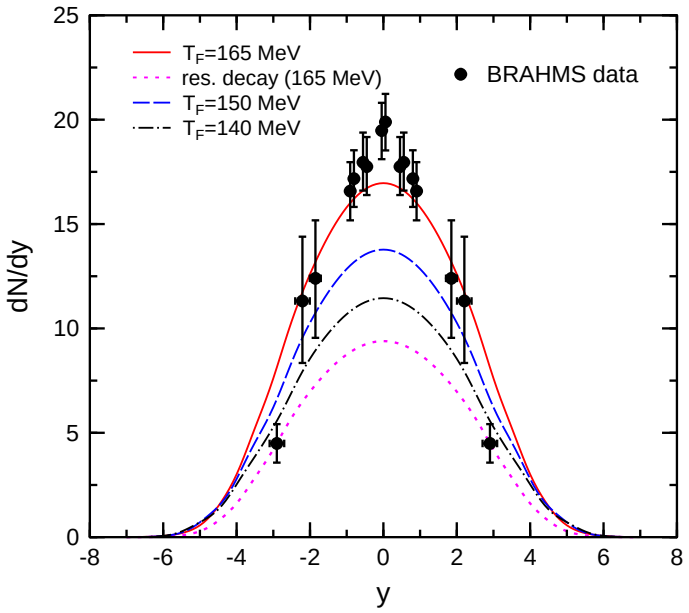

Fig. 3. Same as Fig. 1, but for antiproton rapidity distributions. All results are obtained assuming $\mu_F = 0$. Experimental data are taken from Ref. [26].

It turned out that with the parameter sets from Table 2 can also reproduce reasonably well the antiproton rapidity spectra measured by the BRAHMS Collaboration [26]. Figure 3 shows the antiproton rapidity distributions, calculated for the parameter set C. In this case we explicitly take into account the contribution of the $\overline{\Delta}(1232) \to \pi\overline{p}$ decays, ignoring the width of Δ–isobar. Contributions of higher antibaryon resonances are taken into account in a similar way as for pions and kaons. The resonance contribution reaches about 55% at $T_F = 165\,\mathrm{MeV}$. One should consider these results as an upper bound of the antiproton yield. A more realistic model should include the effects of nonzero baryon chemical potentials which will certainly reduce the antibaryon yield. The thermal model analysis of RHIC data, performed in Ref. [35], gives rather low values for the baryon chemical potentials, $\mu_F \sim 30\,\mathrm{MeV}$, at midrapidity. This will suppress the antiproton yield by about 20%.

We have calculated additionally the rapidity distribution of the total energy

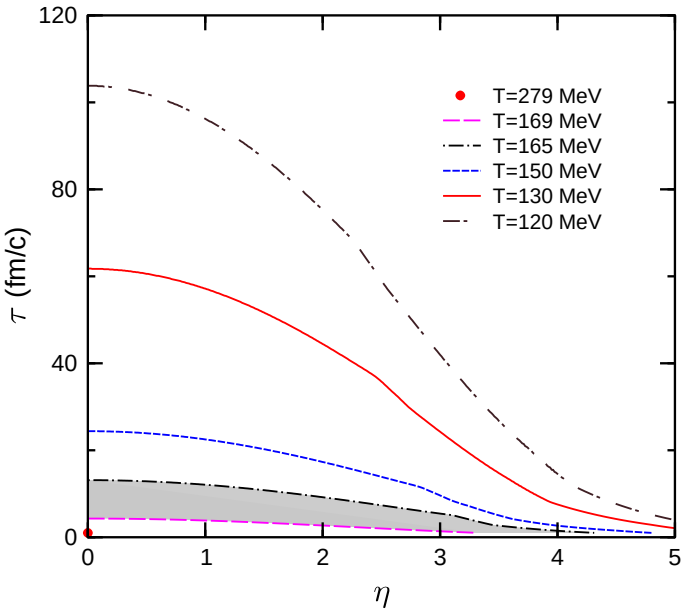

Fig. 4. Isotherms in the $\eta - \tau$ plane calculated for the parameter set C. Only forward hemisphere is shown. Different curves correspond to different values of the freeze–out temperature T_F . Shaded region indicates the mixed phase. The dot near the origin corresponds to maximum temperature at the initial state.

of secondary particles, dE/dy , in order to check the energy balance in the considered reaction. In this calculation we take into account not only direct pions and kaons (charged and neutral), but also heavier mesons and $B\overline{B}$ pairs (the same set of resonances as in the calculation of pion and kaon spectra). The contribution of heavy mesons and $B\overline{B}$ pairs was found in the zero–width approximation for the temperature $T_F = 165\,\mathrm{MeV}$. By integrating dE/dy, we have determined E_1 and E_3, the total energies of secondaries within the rapidity intervals $|y| < 1$ and $|y| < 3$, respectively. The BRAHMS Collaboration estimated $E_{1,3}$ from the rapidity distributions of charged pions, kaons, protons and antiprotons in most central Au+Au collisions at $\sqrt{s_{NN}} = 200\,\mathrm{GeV}$. The values $E_1 \simeq 1.5\,\mathrm{TeV}, \quad E_3 \simeq 9\,\mathrm{TeV}$ have been reported in Ref. [36]. From Table 2 one can see that these values are well reproduced by the model.

Based on the above analysis we conclude that within the hydrodynamical model the BRAHMS data can be well described with the parameters of the initial state ($\tau_0 = 1\,\mathrm{fm/c}$):

$$\epsilon_0 \simeq 9 \pm 1\,\mathrm{GeV/fm}^3, \quad \sigma \simeq 1.5 \pm 0.3, \quad \eta_0 \lesssim 1. \tag{17}$$

These profiles are intermediate between the Landau and Bjorken limits. It is worth noting that the observed pion rapidity distribution can be well approximated by the Gaussian with the width $\sigma_{\mathrm{exp}} \simeq 2.3$ [27]. On the other hand,

the pure Landau model gives for $c_s^2 = 0.15$ a much smaller width $\sigma_{\rm Lan} \simeq 1.38$.

The dynamical evolution of matter as predicted by the present model is illustrated in Fig. 4 where the matter isotherms are shown in the $\eta - \tau$ plane. One can clearly see that the initial stage of the evolution, when matter is in the quark–gluon phase, last only for a very short time, of about 5 fm/c. The region of the phase transition is crossed in less than 10 fm/c. This clearly shows that the slowing down of expansion associated with the "soft point" of the EOS plays no role, when the initial state lies much higher than the phase transition region. In this situation the system spends the longest time in the hadronic phase. The freeze-out at $T_F = 130\,{\rm MeV}$ requires an expansion time of about 60 fm/c at $\eta = 0$. This is certainly a very long time which is seemingly in contradiction with experimental findings. Indeed, the interferometric measurements [37] show much shorter times of hadron emission, of the order of 10 fm/c. This discrepancy can not be removed by considering other EOS or initial conditions. Some reduction of the freeze–out times can be achieved by including the effects of 3D expansion and chemical nonequilibrium [15]. But, probably, a more promising solution would be an explosive decomposition of the quark–gluon plasma, proposed in Ref. [38]. This may happen at very early times, right after crossing the critical temperature line, when the plasma pressure becomes very small or negative. We shall consider this possibility in a forthcoming publication.

In conclusion, we have generalized Bjorken's scaling hydrodynamics for finite–size profiles of energy density in pseudorapidity space. The hydrodynamical equations were solved numerically in $\tau - \eta$ coordinates starting from the initial time $\tau_0 = 1$ fm/c until the freeze–out stage. The sensitivity of the final particle distributions to the initial conditions, the freeze–out temperature and the EOS has been investigated. A comparison of $\pi, K, \overline{p}$ rapidity spectra with the BRAHMS data for central Au+Au collisions at $\sqrt{s_{NN}} = 200\,{\rm GeV}$ has been made. Best agreement with these data is obtained for initial states with a nearly Gaussian profile and maximum energy densities of about 10 GeV/fm^3 at $\tau = 1$ fm/c. The only unsatisfactory aspect of these calculations is the prediction of very long freeze–out times, $\sim 50\,{\rm fm/c}$ for pions.

Finally, we would like to comment on two points. First, it is worth noting that the above–mentioned 2+1 dimensional models [7,8,9,10,11], which assume Bjorken scaling in the beam direction, are apparently not very accurate even for the slice around $\eta = 0$. Indeed, in contrast to the Bjorken model, our calculations for finite size profiles show that the quantity $s(\tau, \eta)\tau$ does not stay constant during the expansion, but it drops by about 15% for $|\eta| < 1$ at large times. Therefore, only full 3D models can provide a realistic description.

Second, one can start the hydrodynamical evolution from an earlier time, i.e. assuming smaller τ_0 . In this case one should choose accordingly higher initial

energy densities. But τ_0 cannot be taken too small, since at very early times the energy is most likely stored in strong chromofields [39]. The quark–gluon plasma is produced as a result of the decay of these fields. Estimates show that the characteristic decay times are in the range $0.3 - 1.0$ fm/c. At earlier times the system will contain both fields as well as produced partons, and the evolution equations are more complicated, see e.g. Ref. [40].

The authors thank I.G. Bearden, J.J. Gaardhøje, M.I. Gorenstein, Yu.B. Ivanov, L. McLerran, D.Yu. Peressounko and V.N. Russkikh for useful discussions. This work was supported in part by the BMBF, GSI, the DFG grant 436 RUS 113/711/0–2 (Germany) and the grants RFBR 05–02–04013 and NS–8756.2006.2 (Russia).

References

[1] L.D. Landau, Izv. Akad. Nauk Ser. Fiz. 17 (1953) 31; in Collected Papers of L.D. Landau, Gordon and Breach, New York, 1965, p. 665.

[2] J.D. Bjorken, Phys. Rev. D 27 (1983) 140.

[3] G.A. Melekhin, Zh. Eksp. Teor. Fiz. 26 (1958) 529 [Sov. Phys.–JETP 8 (1959) 829].

[4] Yu.A. Tarasov, Yad. Fiz. 26 (1977) 770 [Sov. J. Nucl. Phys. 26 (1977) 405].

[5] I.N. Mishustin, L.M. Satarov, Yad. Fiz. 37 (1983) 894 [Sov. J. Nucl. Phys. 37 (1983) 532].

[6] J.P. Blaizot, J.Y. Ollitrault, Phys. Rev. D 36 (1987) 916.

[7] P.F. Kolb, J. Sollfrank, U. Heinz, Phys. Lett. B 459 (1999) 667.

[8] S.A. Bass, A. Dumitru, Phys. Rev. C 61 (2000) 064909.

[9] D.Yu. Peressounko, Yu.E. Pokrovsky, Nucl. Phys. A 669 (2000) 196.

[10] P.F. Kolb, P. Huovinen, U. Heinz, H. Heiselberg, Phys. Lett. B 500 (2001) 232.

[11] D. Teaney, J. Lauret, E.V. Shuryak, Phys. Rev. Lett. 86 (2001) 4783; nucl–th/0110037.

[12] H. Stöcker, J.A. Maruhn, W.Greiner, Phys. Rev. Lett. 44 (1980) 725.

[13] D.H. Rischke, Y. Pürsün, J.A. Maruhn, H. Stöcker, W. Greiner, Heavy Ion Phys. 1 (1995) 309.

[14] C. Nonaka, E. Honda, S. Muroya, Eur. Phys. J. C 17 (2000) 663.

[15] T. Hirano, Phys. Rev. C 65 (2002) 011901(R);
T. Hirano, K. Tsuda, Phys. Rev. C 66 (2002) 054905.

[16] Y. Hama, T. Kodama, O. Socolowski Jr., Braz. J. Phys. 35 (2005) 24.

[17] C. Nonaka, S. Bass, nucl–th/0510038.

[18] A.A. Amsden, A.S. Goldhaber, F.H. Harlow, J.R. Nix, Phys. Rev. C 17 (1978) 2080.

[19] R.B. Clare, D. Strottman, Phys. Rep. 141 (1986) 178.

[20] H.W. Barz, B. Kämpfer, L.P. Csernai, B. Lukacs, Nucl. Phys. A 465 (1987) 743.

[21] I.N. Mishustin, V.N. Russkikh, L.M. Satarov, Yad. Fiz. 48 (1988) 711 [Sov. J. Nucl. Phys. 48 (1988) 454]; Nucl. Phys. A 494 (1989) 595.

[22] U. Katscher, D.H. Rischke, J.A. Maruhn, W. Greiner, I.N. Mishustin, L.M. Satarov, Z. Phys. A 346 (1993) 209.

[23] J. Brachmann, S. Soff, A. Dumitru, H. Stöcker, J.A. Maruhn, W. Greiner, L.V. Bravina, D.H. Rischke, Phys. Rev. C 61 (2000) 024909.

[24] Yu.B. Ivanov, V.N. Russkikh, V.D. Toneev, Phys. Rev. C 73 (2006) 044904.

[25] H. Stöcker, Nucl. Phys. A 750 (2005) 121.

[26] BRAHMS Collaboration, I.G. Bearden et al., Phys. Rev. Lett. 93 (2004) 102301.

[27] BRAHMS Collaboration, I.G. Bearden et al., Phys. Rev. Lett. 94 (2005) 162301.

[28] M. Le Bellac, Thermal Field Theory, Cambridge Press, Cambrige, 1996.

[29] D.H. Rischke, S. Bernard, J.A. Maruhn, Nucl. Phys. A 595 (1995) 346.

[30] J.P. Boris, D.L. Book, J. Comp. Phys. 11 (1973) 38.

[31] F. Cooper, G. Frye, Phys. Rev. D 10 (1974) 186.

[32] J. Sollfrank, P. Koch, U.W. Heinz, Phys. Lett. B 252 (1990) 256;
Z. Phys. C 52 (1991) 593.

[33] H.Bebie, P. Gerber, J.L. Goity, H. Leutwyler, Nucl. Phys. B 378 (1992) 95.

[34] Particle Data Group, S. Eidelman et al., Phys. Lett. B 592 (2004) 1.

[35] A. Andronic, P. Braun–Munzinger, Lect. Notes Phys. 652 (2004) 35.

[36] BRAHMS Collaboration, J. Arsene et al. Nucl. Phys. A 757 (2005) 1.

[37] STAR Collaboration, C. Adler et al., Phys. Rev. Lett. 87 (2001) 82301.

[38] I.N. Mishustin, Phys. Rev. Lett. 82 (1999) 4779.

[39] L. McLerran, R. Venugopalan, Phys. Rev. D 49 (1994) 2233.

[40] I.N. Mishustin, J.I. Kapusta, Phys. Rev. Lett. 88 (2002) 112501.